

Semantic Exploration and Dense Mapping of Complex Environments using Ground Robots Equipped with LiDAR and Panoramic Camera

Xiaoyang Zhan, Shixin Zhou, Qianqian Yang, Yixuan Zhao,
Hao Liu, Srinivas Chowdary Ramineni and Kenji Shimada

Abstract—This paper presents a system for autonomous semantic exploration and dense semantic target mapping of a complex unknown environment using a ground robot equipped with a LiDAR-panoramic camera suite. Existing approaches often struggle to strike a balance between collecting enough high-quality observations from multiple view angles and avoiding unnecessary repetitive traversal. To fill this gap, we propose a complete system that combines mapping and planning. We first redefine the task as completing both geometric coverage and semantic viewpoint observation. Subsequently, we manage semantic and geometric viewpoints separately and propose a novel Priority-driven Decoupled Local Sampler to generate local viewpoint sets. This allows for explicit multi-view semantic inspection and voxel coverage without unnecessary repetition. Building on this, we develop a hierarchical planner that ensures efficient global coverage. In addition, we propose a Safe Aggressive Exploration State Machine, which allows aggressive exploration behavior while ensuring the robot’s safety. Our system includes a plug-and-play semantic target mapping module that integrates seamlessly with state-of-the-art SLAM algorithms for pointcloud-level dense semantic target mapping. We validate our approach through extensive experiments in both realistic simulations and complex real-world environments. Simulation results demonstrate that our planner achieves faster exploration and shorter travel distances while guaranteeing a specified number of multi-view inspections. Real-world experiments further confirm the effectiveness of the system in achieving accurate dense semantic object mapping of unstructured environments.

I. INTRODUCTION

With the growing success of autonomous exploration algorithms, their applications are drawing increased attention from the research community. Semantic exploration is particularly important in scenarios such as factories and construction sites. Unlike unmanned aerial vehicles (UAVs) commonly used in prior work, ground robots offer the advantage of accommodating more powerful sensors and computing systems, including high-resolution LiDAR and panoramic camera arrays. This paper focuses on semantic exploration and mapping for ground robots.

Despite advancements, autonomous semantic exploration faces challenges. First, it requires an effective integration of mapping and planning, as the planner depends on semantic information to make informed decisions. To achieve high-quality mapping, the planner needs to collect comprehensive measurements from multiple distinct viewpoints while computing a path for geometric coverage that is as short as



Fig. 1. A real-world semantic exploration experiment in a lobby environment. (a) Lobby scene with legged robot. (b) Visualization showing background map, dense object map, and exploration path. Green boxes mark semantic objects (chairs) with highlighted dense maps. (c)-(e) Sample dense target maps. Full results in Secs V-D.

possible. Existing methods either assign semantic weights to potential exploration goals that prioritize positions near target objects [1][2] or sample viewpoints that cover unknown regions [3]. However, the former often causes repetitive movements around objects, while the latter neglects the importance of complete and diverse observation from multiple view angles for target objects. There is still a lack of a planner that strikes the balance for both. Another difficulty is that robots operating in complicated environments need to balance exploration speed and collision risks. Existing planners often limit exploration to known free spaces for safety, but this over-conservative strategy results in short-sighted decisions and inefficient paths [4]. However, aggressive exploration in unknown areas raises collision risks, especially at higher speeds, which limits planner performance.

To address the above challenges, this paper proposes a system that performs semantic exploration planning and dense semantic target mapping in an unknown environment. We develop a modular, object-centric semantic target dense mapping component that works seamlessly with various state-of-the-art SLAM systems. The planning component defines the semantic exploration task as inspecting all unknown voxels and visiting evenly distributed semantic viewpoints to ensure high-quality mapping. To support the integration between mapping and planning, we introduce a hierarchical planner that manages semantic viewpoints and geometric exploration viewpoints in a unified framework. We propose a novel Priority-driven Decoupled Local Sampler to handle the two

types of viewpoints separately and generate a minimum set of viewpoints that supports the completeness of both semantic and geometric coverage tasks. The sampler is then integrated with a global planner to generate the global optimal path by solving an asymmetric traveling salesman problem (ATSP). After that, to support aggressive exploration, a novel Safe Aggressive Exploration State Machine is proposed to ensure aggressive and resilient exploration in crowded regions.

In summary, this work has the following contributions:

- A *plug-in semantic target mapping module based on LiDAR-Panoramic camera fusion*, tailored to the semantic exploration planner. This module can be integrated with any state-of-the-art SLAM system.
- A *novel Priority-driven Decoupled Local Sampler* that manages the semantic and geometric viewpoints in a decoupled manner and generates a viewpoint set for global path planning.
- An *aggressive exploration state machine* that supports the robot in choosing aggressive goals, maintaining safety in unknown space, and recovering from the near collision state.
- A *complete ground robot system* with a specialized sensor suite, modular mapping pipeline, and a novel planning framework. Simulated and real-world tests in industrial and construction environments validate the effectiveness of the system.

II. RELATED WORK

Autonomous robot exploration has made great progress over the decades [5][6][7][8]. One stream of methods is based on frontiers, which are the boundaries between free space and unknown space. Yamauchi [5] greedily chooses the closest frontier as the next goal, while later methods [6][9] apply more sophisticated frontier clustering, viewpoint generation, and path planning techniques. Another stream of methods is based on Next-Best-View (NBV) and graph sampling, such as RRT or PRM. In [10], a graph is built by sampling in safe free space and calculating the information gain for each node. The next best node with the highest average gain is chosen as the next goal. Later, Dang et al. [8] propose rapidly-exploring random graphs for more rapid NBV exploration planning, and other methods [11][12][13][14][15] continue to propose more carefully designed utility functions for information gain and graph structures. In recent years, more algorithms have been formulated the traveling salesman problem (TSP)[6][7][16][3] to improve the efficiency of traversing all viewpoints or graph nodes.

At the same time, the SLAM community has an increasing interest in metric-semantic SLAM. Some of them use sparse representations such as cubes [17], ellipsoids [18], or combinations of geometric shapes [19], and combine the parameters into a factor graph to formulate an optimization problem. Others use dense representations such as meshes [20] or sufels [21].

With the development of both areas, exploration with semantic objects is gaining more attention. Tung et al. [2] define an object gain function to handle re-observation from

multiple resolutions, and Sotiris et al. [1] propose multiple utility functions to include both background and object information gain to improve the quality of camera-based mesh reconstruction. Yiming et al. [3] further propose a hierarchical planning framework to solve exploration with target search. At the same time, the DARPA subterranean challenge facilitated semantic exploration research. Xianmei et al. [22] propose a whole pipeline to guarantee high precision and recall of semantic detection during exploration and emphasize the importance of observation from multiple view angles. Graeme et al. [23] utilized the fusion of multiple sensors during exploration and mapping.

None of these methods, however, explicitly defines multi-view observation viewpoints for object mapping in exploration, thus suffering from randomness due to unnecessary re-observation or inadequate observation. In addition, most algorithms are still based on the greedy NBV strategy with semantic weights, lacking careful consideration of global optimality. Our method fills this gap by explicitly defining the semantic viewpoint with a certain density around target objects while enabling efficient traversing considering both geometric coverage and semantic observation. Furthermore, we developed a Safe Aggressive State Machine to support aggressive exploration in complicated real-world environments.

III. PROBLEM FORMULATION

The goal of this paper is to enable a single ground robot, equipped with a LiDAR and panoramic camera fusion system, to autonomously plan its trajectory within an unknown environment and accurately map both the environment itself and specified target objects of interest. The robot should generate a dense point cloud for both the environment and the identified objects, while optimizing trajectory efficiency to ensure timely completion of the mapping tasks.

A. Robot and Sensor Model

In this work, we employ the Boston Dynamics Spot as a quadruped mobile platform equipped with a specialized sensor system. The sensor suite includes an Ouster OS-1-128 LiDAR and a panoramic camera system. The LiDAR features a 45° vertical field of view (FOV) and a 360° horizontal FOV, with 128 vertical channels, operating at a frequency of 10 Hz. The panoramic camera system is the Boston Dynamics CAM Payload, which integrates data from five Sony IMX290 cameras to provide a 360° × 165° field of view.

B. Environment Model

The unknown environment is modeled as a bounded 3D volume $V \subset \mathbb{R}^3$, discretized into individual voxels v . Each voxel v is associated with an occupancy probability $P_o(v)$. Before receiving any sensor measurements, each voxel is initialized as *unknown* with $P_o(v) = 0.5$. Through the accumulation of sensor measurements and subsequent ray-casting, voxels are eventually classified as either *occupied* V_{occ} or *free* V_{free} . However, due to the complexity of environment geometry, robot configuration constraints, and sensor limitations, some residual voxels V_{res} may remain

unmapped. Hence, the relationship $V_{free} \cup V_{occ} \cup V_{res} = V$ holds at the end of the exploration.

C. Problem Definition

Given the robot, sensor, and environment models, the overall problem can be defined as:

Problem 1 (Semantic Target Mapping): Assume an unknown number $N \subset \mathbf{N}$ of target objects, each associated with a semantic label λ from a semantic label set \mathbb{L} . The robot must detect and classify all target objects, extracting the dense point cloud for both the target objects and the surrounding environment.

As discussed in Section I, the semantic exploration task must consider both target object observation and geometric coverage. We divide the space centering around a target object O_i with radius r into M evenly distributed sectors. Each sector S_m^i is defined as an *observation space*. Then, we define the semantic exploration task as follows:

Problem 2 (Semantic Exploration): Given the sensor model and configuration ψ_{robot} , plan a path σ_{robot} starting from an initial configuration ξ_{robot} such that: (1) it covers at least one valid detection in every observation space S_m^i for any target object O_i , whenever possible; and (2) it observes all voxels so that $V_{free} \cup V_{occ} = V \setminus V_{res}$.

IV. METHODOLOGY

The proposed system comprises a plug-in semantic mapping module and a hierarchical planner, as shown in Fig. 2. The mapping module, discussed in Section IV-B, takes as input the panoramic image \mathbf{I} , LiDAR point cloud \mathbf{P} , and odometry \mathbf{O} , then outputs the dense point cloud map of both background environment \mathbf{M}_B and target objects \mathbf{M}_O . Concurrently, the hierarchical planner generates the exploration path that ensures both semantic observation and geometric coverage. Section IV-C describes how the Priority-driven Decoupled Sampler decouples semantic observation and geometric coverage and chooses a set of both geometric and semantic viewpoints. Subsequently, Section IV-D explains how the global planner optimizes the travel path through viewpoints. Finally, a Safe Aggressive Exploration State Machine is proposed in Section IV-E to enable efficient but safe exploration.

A. Sensor Fusion and Pre-processing

Given the input measurement from both LiDAR and panoramic image, they are associated by:

$$I_x = \frac{W_{img} (-\text{atan2}(Y, X) + \pi)}{2\pi}, \quad (1)$$

$$I_y = f_y \left(-\frac{Z}{\sqrt{X^2 + Y^2}} \right) + y_0, \quad (2)$$

where W_{img} is the image width, X, Y, Z are the 3D point input from the LiDAR frame, f_y is the vertical focal length of the panoramic camera, and y_0 is the vertical coordinate of the panoramic image's principal point, I_x and I_y are the associated coordinates in the panoramic image frame.

Using Eq. 1, 2, odometry, and object 2D detection, a raw point cloud is extracted for each instance mask of the object. Then, it is processed by applying DBSCAN clustering, selecting the closest group to the observation pose, and filtering out points lower than the ground. The instance mask, the associated instance point cloud, and the pose estimation at the current time step are packaged as a measurement z .

B. Modular Semantic Target Mapping

Our plug-in semantic target mapping module builds a coarse-to-fine object-centric voxel model for each target object, updates the model constantly by real-time input measurement, and extracts a dense point cloud from the background SLAM algorithm.

1) *Data Association:* Upon receiving a processed point cloud, the module matches it to existing object models using the bounding box intersection-over-union (IOU). If the best IOU falls below a threshold T_{iou} , a new object model is initialized.

2) *Model Update:* The object model periodically incorporates new observations and processes multi-view observations statistically, accounting for potential false positives/negatives from varying view angles. Specifically, for each object model O_i , observations are grouped into n observation sets. Each set corresponds to the observation space defined in *Problem 2*. Within each observation set,

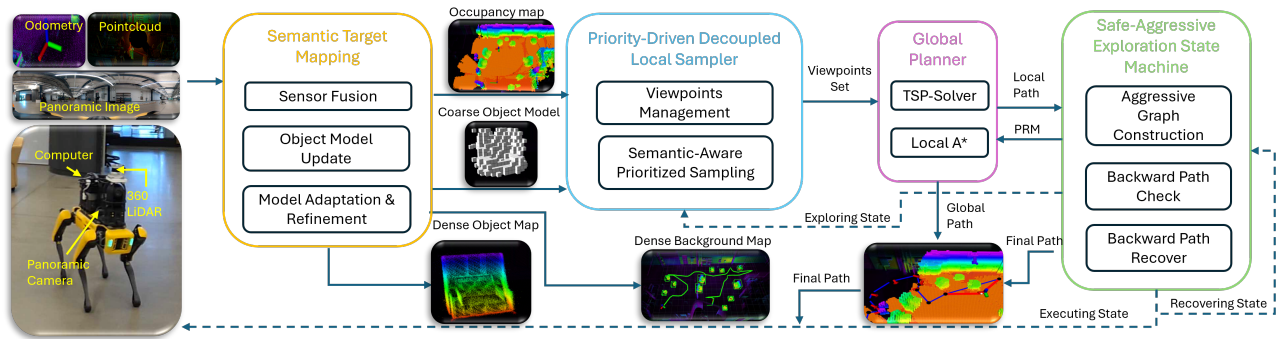


Fig. 2. System overview: The system processes odometry, LiDAR, and panoramic image inputs. The mapping module builds object-centric models, occupancy, and dense maps. The planner samples viewpoints based on these maps, creates local viewpoint sets in active regions, and generates optimal paths. The Safe-Aggressive Exploration State Machine maintains aggressive graph construction (AGC) while supporting recovery from pseudo-collision.

the model retains a keyframe measurement z_i^n and stores its corresponding mask m_i^n and pose estimation p_i^n . The key frame measurement z_i^n is selected by the measurement with the highest *mask score*, defined as the following:

$$S_{mask} = IOMax(V_{mask}, V_{model}) * V_{mask}, \quad (3)$$

where V_{mask} and V_{model} are bounding box volumes of the mask and current model, respectively. IOMax is the intersection over the maximal box. This score prioritizes masks giving more complete object measurement while avoiding taking an over-segmented point cloud with an unexpectedly large size.

However, false positive detection due to a complicated background could also produce a false positive keyframe measurement. To account for this, we model the validity of keyframes as a Bernoulli random variable. The optimal estimation of probability is given by the number of valid detections over the total number of observations in this observation set, where a valid observation means a mask score greater than a threshold T_{score} . Only keyframes with a true positive probability greater than T_p will be kept. Each accepted observation is integrated into the voxel model, updating per-voxel probabilities. After this, for each observation set, the object model is ray-cast back to the key frame mask m_i^k taking occlusions into account. The voxels outside the mask decrease its probability by p_{dec} , while those inside the mask increase the probability by p_{inc} . The above process is repeated for all observation sets.

3) *Map Adaptation and Refinement*: Errors in the data association process can lead to two common issues: a single object’s measurements being split across different object models, or measurements from two different objects being assigned to the same object model. We propose two strategies to address these issues: model merging and model re-centering. For the former case, model merging is applied when two object models have an Intersection over Minimum (IoMin) greater than a threshold T_{IOM} . In this scenario, their data are merged to form a new object model. The probabilities of belonging to the object model are averaged, and the observation sets and key frames from both models are concatenated. To address the latter case, we apply model re-centering. During each model update iteration, both the geometric center and the center of mass are recalculated. If the distance between the two exceeds a threshold T_{doc} , the model is re-centered to its center of mass, discarding any information outside the new map boundary. This adjustment helps to “pull back” the model when incorrect measurements have been associated and have biased the map. After finishing all these steps, the dense point cloud from LiDAR SLAM will be registered and stored in each voxel of a model. Filtering out voxels with too sparse a point cloud, which could be noise, a dense object map is extracted.

C. Priority-driven Decoupled Local Sampler

During each planning iteration, only active exploration regions that contain uncovered frontiers are considered. Among these, the local sampler is invoked only for regions that

intersect with the robot’s Local Planning Horizon (LPH), selecting suitable viewpoints for exploration, as illustrated in Fig. 3(a). This section is divided into two parts: the first describes the generation, updating and management of semantic and geometric viewpoints; the second explains how to construct a set of viewpoints that collectively cover the local exploration region and its associated observation spaces.

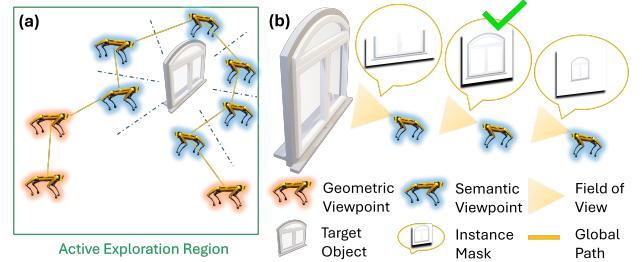


Fig. 3. Overview of Priority-driven Decoupled Local Sampler. (a) Sampling semantic viewpoints and geometric viewpoints in a local active exploration region. (b) Semantic viewpoints sampling along one observation space. The viewpoint with the best observation score (2nd viewpoint from left to right) is selected. Viewpoint with incomplete observation (1st viewpoint from left to right) is invalid.

1) *Semantic and Geometric Viewpoint Management*: As described in Sections III-C and IV-B, the robot must observe targets from all accessible observation spaces. To achieve this, semantic viewpoints are sampled along the centerline of each observation space at a fixed spatial resolution, as shown in Fig. 3(b). For each center line, the candidate viewpoint with the highest observation score is selected. The score is calculated by projecting the object model into the camera frame and taking the area of the model’s mask. To ensure observation quality and completeness, two types of viewpoints are discarded: (a) those resulting in occluded object observations, and (b) those yielding incomplete object observations, determined via ray-casting from the current pose. In case (b), an additional viewpoint is sampled along the same direction with one higher resolution increment. If case (b) occurs, the sampler will sample an additional viewpoint along the same direction with one more resolution increment. Viewpoints are dynamically updated following two rules: (a) If the robot passes by an observation space and reaches an observation score above a threshold T_{obs} , the corresponding viewpoint is removed; and (b) If a viewpoint falls into a voxel that changes from unknown to occupied, it is discarded and resampled along the centerline.

After updating, the sampled viewpoints are registered in a 2D grid with resolution g , with each grid cell assigned to its corresponding active exploration region. The planner considers only the grid centers as viewpoints. This reduces redundant visits to nearby viewpoints—especially those associated with different objects—while maintaining sufficient multi-view coverage.

Geometric viewpoints are obtained using a hierarchical Probabilistic RoadMap (PRM). At the lower level, a dense

PRM is constructed to support fine-grained local path planning. At the higher level, nodes are selectively sampled from the dense PRM to serve as geometric viewpoints. Each node is assigned an information gain (IG) score, defined as the number of unknown voxels visible from its pose, given the sensor model. To improve efficiency, IG is approximated using sparse ray-casting.

2) *Semantic-Aware Prioritized Sampling*: The sampling of geometric and semantic viewpoints must address two key factors: the potential mutual overlap between viewpoints (known as the submodularity property [7]) and the need for specific semantic viewpoints for object observation. To account for these, we propose a semantic-prioritized sampling mechanism incorporating viewpoints’ mutual overlap into consideration. Our approach begins by adding all frontiers within the current exploring region to a frontier queue. To ensure effective multi-view observation, our sampler gives precedence to semantic viewpoints, pushing them to the viewpoints queue and calculating their frontier coverage. The covered frontiers are then removed from the queue. Subsequently, geometric viewpoints receive NBV-reward values based on expected information gain over time.:

$$R_{nbv}^k = \frac{\sum_{i=1}^n IG_i}{\sum_{i=1}^n T_{i-1,i}}, \quad (4)$$

$$T_{i-1,i} = \frac{\arctan\left(\frac{y_i - y_{i-1}}{x_i - x_{i-1}}\right)}{\omega} + \frac{\|n_i, n_{i-1}\|_2}{v}, n_i \in \sigma_k, \quad (5)$$

where σ_k is the planned path to viewpoint k , comprising n nodes n_i . IG_i is the information gain of n_i , $T_{i-1,i}$ is the estimated travel time from n_{i-1} to n_i . ω and v are the expected angular and linear velocity.

All geometric viewpoints are pushed into an NBV-reward priority queue and are sampled in descending order. Each viewpoint undergoes pseudo-sampling, where the sampler applies its sensor model to estimate frontier coverage. The sampler accepts viewpoints with significant incremental coverage, applying their effects to the frontier queue while dropping those with minimal impact. The process terminates when either the reward queue is empty or the current sample’s reward becomes negligible.

D. Global Planner

The global planner routes through all active regions containing uncovered frontiers, operating in a Receding-Horizon approach—executing only one global step before recalculating. We formulate this as an Asymmetric Traveling Salesman Problem (ATSP) where nodes represent viewpoints sampled by the local sampler. The cost matrix \mathbf{C} has the dimension of $(N + 1, N + 1)$, where N is the number of viewpoints. Each entry \mathbf{C}_{ij} represents the traveling time cost from Viewpoint i to Viewpoint j :

$$\mathbf{C}_{i,j} = \mathbf{C}_{j,i} = t_{est}^{i,j}, i, j \in \{1, 2, \dots, N\}, \quad (6)$$

where $t_{est}^{i,j}$ is the estimated travel time cost from viewpoint i to viewpoint j . Unlike traditional approaches, we use different cost metrics for different viewpoints. Since the

Algorithm 1: Safe-Aggressive Exploration State Machine

Input: $\eta \in \{exploring, recovering, executing\}$

```

1 if  $\eta = exploring$  then
2   AggressiveGraphConstruction()
3    $success, \sigma_{path} \leftarrow \mathbf{exploreReplan}()$ 
4   if  $success$  then
5      $\eta \leftarrow executing$ 
6   else
7      $\eta \leftarrow recovering$ 
8 else if  $\eta = executing$  then
9    $safe \leftarrow \mathbf{backwardPathCheck}()$ 
10  if not  $safe$  then
11     $\eta \leftarrow exploring$ 
12 else if  $\eta = recovering$  then
13  backwardRecover()
14   $\eta \leftarrow exploring$ 

```

global path is executed in a Receding-Horizon manner, only the first segment is executed precisely. The travel time from the current position to the k^{th} viewpoint is computed as:

$$\mathbf{C}_{0,k} = t_{est}^{0,k} = \sum_{i=1}^n T_{i-1,i}, \quad (7)$$

where n is the number of nodes in short-cut path found by A^* .

However, since most viewpoints are located in an unknown space, their shortest paths cannot be precisely determined and may never be executed. Therefore, the planner employs Euclidean Distance to evaluate travel cost:

$$\mathbf{C}_{i,j} = t_{est}^{i,j} = c * \frac{\|VP_i, VP_j\|_2}{v}, i \neq 0, j \neq 0 \quad (8)$$

where VP is the viewpoint, c is a time-cost-coefficient. Since the TSP typically involves a closed loop, but exploration requires an open path, the planner creates a virtual loop by assigning zero cost from any viewpoint back to the current position, formulating an ATSP:

$$\mathbf{C}_{k,0} = 0. \quad (9)$$

After solving the global path, only the segment to the first goal is executed. The planner then replans until all viewpoints in active regions are covered, marking the end of exploration.

E. Safe Aggressive Exploration State Machine

Traditional planners restrict goals and paths to known free space for safety, but they lead to short-sighted goal selection. Conversely, naively assuming unknown space is traversable risks instability through overshooting or “pseudo-collisions” (false collision perceptions causing unexpected halts). To balance speed and safety, we propose an Aggressive Exploration State Machine with three states: $\{exploring, executing, recovering\}$, maintaining planning continuity while allowing rapid exploration.

(1) In the *exploring* state, the planner aggressively constructs and dynamically maintains a locally safe PRM graph by Aggressive Graph Construction (AGC). It samples nodes

in both unknown and free space, assuming that all non-occupied edges are valid. The planner performs A* path search and shortcuts using this same aggressive assumption. We adopt an adaptive PRM sampling strategy following [24] that prioritizes areas with sparse nodes. As the robot moves, the planner dynamically updates the dense PRM by identifying newly occupied nodes, removing them along with their neighbors and edges inside the LPH at a certain frequency. Unlike [14], our approach dynamically updates the PRM to account for mistaken assumptions about unknown space, maintaining a locally safe PRM during aggressive sampling. Upon finding a valid exploration path, the system transitions to the *executing* state. Otherwise, the system identifies a "pseudo collision" and enters the *recovering* state.

(2) During *executing* state, the system conservatively verifies whether the path and its surrounding areas (within a safe distance) consist of actual free space, checking in backward order. If deemed unsafe, the system reverts to the exploring state to generate a new path.

(3) In the *recovering* state, we propose a backward recovery mechanism to guide the robot away from the pseudo-collision point and resume exploration. Once the recovery state is activated, the robot backtracks along its last valid exploration path. To ensure that it retreats to a sufficiently distant location, the robot iteratively extends the recovery trajectory backward until it reaches a predefined threshold T_{back} . Simultaneously, the *exploring* state is reactivated in parallel to proactively plan a new exploration path.

V. EXPERIMENTS AND RESULTS

A. Implementation Details

We configure exploration parameters based on environment scale: 15 m grid size with 8 m LiDAR effective range for large-scale simulations, 5 m grid and 3.5 m range for construction sites, and 10 m grid with 5.0 m range

for lobby scenarios. All setups use $N=8$ viewpoints, 0.1 m resolution for occupancy maps and coarse object models, and FAST LIO2[25] for dense point cloud mapping.

TABLE I
BENCHMARKING EXPLORATION PERFORMANCE IN VARIOUS SCENES

Scene	Metric	Semantic Eight	HIRE Semantic	Ours
Office	Runtime (s)	536.2 ± 81.1	613.7 ± 59.5	326.1 ± 11.3 ✓
	Path-length (m)	370.7 ± 46.8	380.6 ± 34.6	197.6 ± 6.2 ✓
	Map(%)	94.7 ± 0.4	96.3 ± 0.8 ✓	95.3 ± 1.0 ✓
	Viewpoints (%)	99.6 ± 0.8	97.3 ± 3.7	100.0 ± 0.0 ✓
Warehouse	Runtime (s)	1092.0 ± 72.7	1287.0 ± 194.9	690.5 ± 30.3 ✓
	Path-length (m)	738.6 ± 58.3	1013.2 ± 144.9	444.1 ± 20.4 ✓
	Map (%)	93.3 ± 1.8	94.2 ± 0.3	94.6 ± 0.7 ✓
	Viewpoints (%)	97.1 ± 2.0	100.0 ± 0.0 ✓	100.0 ± 0.0 ✓
Factory	Runtime (s)	1110.9 ± 119.8	1247.1 ± 215.2	840.2 ± 32.8 ✓
	Path-length (m)	693.5 ± 108.8	858.4 ± 154.0	519.5 ± 55.2 ✓
	Map (%)	94.8 ± 0.16	96.4 ± 0.8 ✓	95.9 ± 0.98
	Viewpoints (%)	97.5 ± 5	98.1 ± 2.3	100.0 ± 0.0 ✓

Map(%) means the percentage of map coverage. View(%) is the percentage of observed semantic viewpoints over total number of expected semantic viewpoints.

B. Benchmark Comparisons

To evaluate the performance of our hierarchical planner, we performed benchmark experiments in three realistic industrial environments in Isaac Sim: 1) Office ($40 \times 40 \times 5$ m) with 13 chairs as target objects, Warehouse ($40 \times 60 \times 5$ m) with 9 forklifts as target objects and Factory ($45 \times 70 \times 5$ m) with 11 robot arms and forklifts as target objects. To demonstrate cross-platform applicability, we used a Husky UGV with a velocity range of 0.5 m/s to 2.2 m/s. The robot is equipped with one LiDAR and two cameras (front and rear) to simulate 360° sensing. To isolate planning performance, we assume ground-truth 3D object detections.

We compared our approach with HIRE, a recent fast exploration algorithm [14], and Semantic Eight [1], a recent

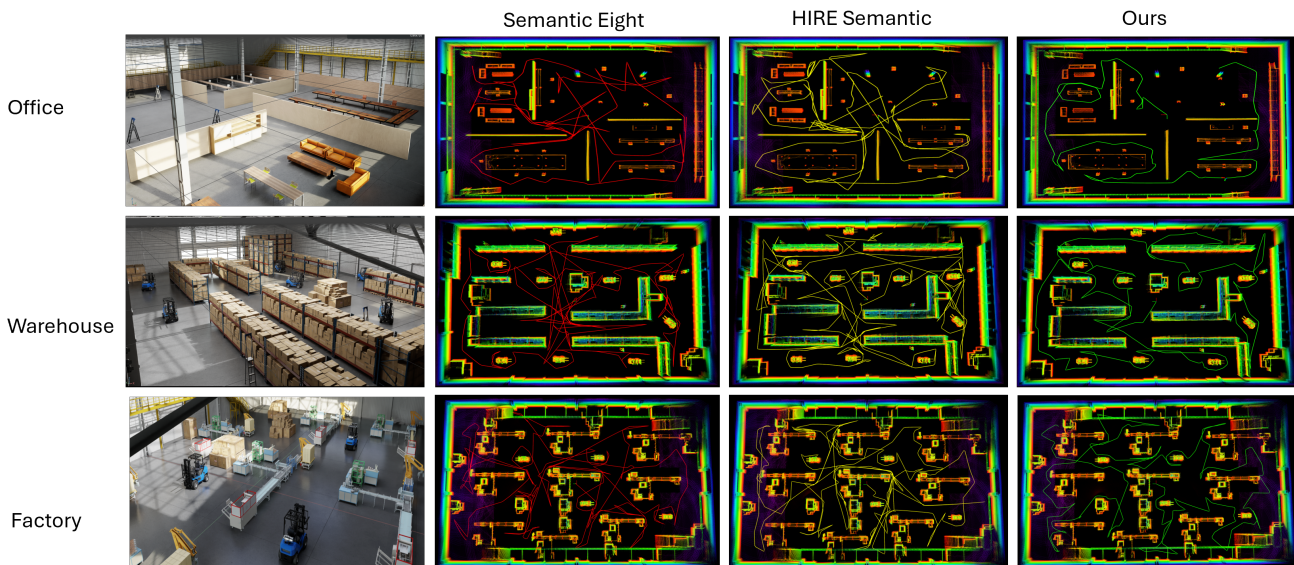


Fig. 4. Exploration trajectories of various methods in all three simulator environments. Our method produces more consistent coverage paths with fewer redundant revisits, demonstrating higher exploration efficiency.

semantic exploration algorithm. To ensure fairness and adapt their metrics to align with our task definition, we enhanced HIRE with a semantic weighting scheme where information gain is calculated as the sum of spatial IG and the semantic gain derived from unvisited visible voxels. Since Semantic Eight was originally designed for depth cameras and tightly integrated with a camera-based SLAM system, we re-implemented its planner to suit our LiDAR-based sensor configuration. Each experiment was repeated five times in each environment. As outlined in Table I, our planner consistently outperformed HIRE, achieving faster exploration times, shorter path lengths, and reduced standard deviations, indicating greater robustness. The trajectory visualizations in Fig. 4 confirm that our method shows a much more consistent and efficient trajectory to finish the coverage with less redundancy across all three scenes.

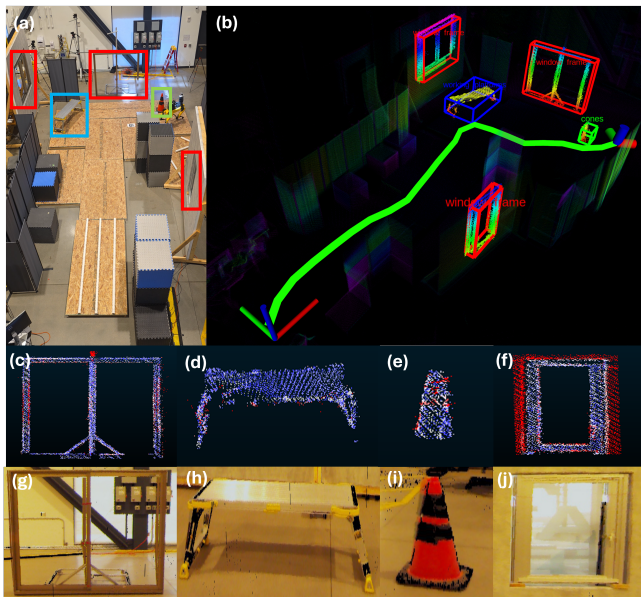


Fig. 5. Overview of the construction site scene and mapping results. (a) Bird’s-eye view of the scene with labeled semantic targets. (b) Final map and robot trajectory. (c)-(f) Dense object map with error heatmaps (blue: low error, red: high error). (g)-(j) Ground-truth target object point cloud. Red boxes: window frames; blue: working platform; green: traffic cone.

C. Ablation Study

We conducted an ablation study in three environments to evaluate the effectiveness of our Safe Aggressive Exploration State Machine, consisting of two key components: Aggressive Graph Construction (AGC) and the Safe State Machine (SM). We evaluated how AGC improves exploration efficiency, how naive AGC without SM falls into collision, and how SM ensures the safety of AGC. As shown in Table II, comparing columns 3 and 5 demonstrates that AGC significantly reduces the path length and decreases the time cost in most scenarios, confirming its contribution to improved planner efficiency. In the Factory scene, the AGC+SM strategy produces a slightly longer time but shorter path length. This occurs because Factory is so crowded and

complicated that aggressive goal selection triggers lots of stops and recoveries, costing more time than conservative behavior. Furthermore, a comparison between columns 3 and 4 shows that using AGC without SM results in failures during long-term exploration in cluttered environments, underscoring the critical safety role of the SM component.

TABLE II
ABLATION STUDY OF SAFE AGGRESSIVE EXPLORATION STATE MACHINE

Scene	Metric	AGC+SM	Only AGC	Only SM
Office	Time (s)	326.1 ± 11.3 ✓	175.8 [†]	433.7 ± 26.9
	Path (m)	197.6 ± 6.2 ✓	89.1 [†]	270.7 ± 30.0
	Map (%)	95.3 ± 1.0	52.8 [†]	96.1 ± 0.3 ✓
	View (%)	100.0 ± 0.0 ✓	50.8 [†]	100.0 ± 0.0 ✓
Warehouse	Time (s)	690.5 ± 30.3 ✓	343.1 [†]	742.2 ± 77.9
	Path (m)	444.1 ± 20.3 ✓	219.2 [†]	469.2 ± 53.7.4
	Map (%)	94.6 ± 0.7 ✓	66.5 [†]	93.6 ± 1.2
	View (%)	100.0 ± 0.0 ✓	55.1 [†]	100.0 ± 0.0 ✓
Factory	Time (s)	840.2 ± 32.8	327.2 [†]	813.5 ± 28.5 ✓
	Path (m)	519.5 ± 55.2 ✓	205.2 [†]	542.8 ± 43.9
	Map (%)	95.9 ± 0.98	52.3 [†]	96.4 ± 1.3 ✓
	View (%)	100.0 ± 0.0 ✓	34.4 [†]	100.0 ± 0.0 ✓

[†] is the mean value from incomplete runs; the system did not successfully complete in any trial.

D. Physical Experiments

We conducted real-world experiments in two environments—a mock construction site and a workspace lobby—using the Boston Dynamics SPOT robot, with the hardware configuration detailed in Section III. A ROG NUC mini PC equipped with an NVIDIA RTX 4070 GPU was mounted on the robot to perform all the computations.

In the 12 m × 8 m mock construction site with 5 semantic targets (3 window frames, 1 work platform, and 1 cone), we used YOLOv7 pre-trained on construction data [26] for object detection and SAM2[27] for segmentation. The robot navigated at an average speed of 0.7 m/s (linear) and 0.4 rad/s (angular), completing the exploration in 54 seconds. Fig. 5(b) shows the trajectory and the overall point cloud, including the dense background and reconstructed semantic objects. Figs. 5(c)-(j) present the comparisons between reconstructed and ground-truth objects. The system achieved 87.19% object map completeness (points within 2.5 cm of the ground truth) with an average error of 3.11 cm, and 99.19% background map completeness with a 2.27 cm error.

In the 12 m × 23 m lobby with 11 chairs of diverse types as semantic targets, the exploration was completed in 132 seconds at 0.9 m/s (linear) and 0.6 rad/s (angular). the robot followed a consistent trajectory that efficiently covered the environment and ensured the observation of all the viewpoints of the targets (Fig. 1). Fig. 6 presents the reconstructed objects and the error analysis. The object map achieved 97.28% completeness with an average error of 1.75 cm, while the background map reached 99.33% completeness and 2.31 cm average error.

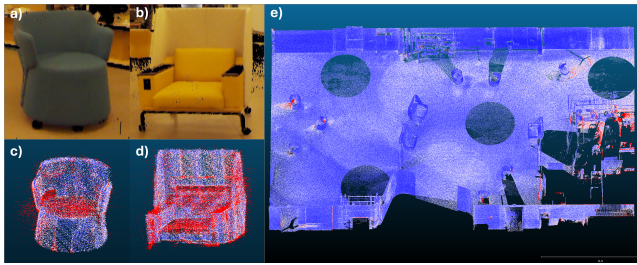


Fig. 6. Mapping results and error visualization for the lobby scene. (a)-(b) Ground-truth point clouds of two example chairs. (c)-(d) Reconstructed point cloud with error heatmaps. (e) Scene-wide error heatmap comparing reconstruction to ground truth. The error increases from blue, white to red.

VI. CONCLUSIONS

This paper presents a comprehensive system for autonomous semantic exploration and dense semantic target mapping. To address the challenge of balancing observation quality and exploration efficiency, we propose a hierarchical planning architecture that handles semantic and geometric viewpoints explicitly while considering their mutual impact, a safe-aggressive exploration state machine that supports aggressive strategy, and a modular mapping component that achieves accurate and complete semantic target mapping utilizing off-the-shelf SLAM algorithms. Extensive simulation experiments validate the planning efficiency, while two real-world deployments demonstrate the system's ability to achieve accurate and complete semantic mapping with minimal exploration overhead. Future work could extend the system to heterogeneous-robots collaboration.

ACKNOWLEDGMENT

This work was supported in part by YKK AP Inc. The authors gratefully acknowledge their support.

REFERENCES

- [1] S. Papatheodorou, N. Funk, D. Tzoumanikas, C. Choi, B. Xu, and S. Leutenegger, "Finding things in the unknown: Semantic object-centric exploration with an mav," in *2023 IEEE International Conference on Robotics and Automation (ICRA)*, 2023, pp. 3339–3345.
- [2] T. Dang, C. Papachristos, and K. Alexis, "Autonomous exploration and simultaneous object search using aerial robots," in *2018 IEEE Aerospace Conference*, 2018, pp. 1–7.
- [3] Y. Luo, Z. Zhuang, N. Pan, C. Feng, S. Shen, F. Gao, H. Cheng, and B. Zhou, "Star-searcher: A complete and efficient aerial system for autonomous target search in complex unknown environments," *IEEE Robotics and Automation Letters*, vol. 9, no. 5, pp. 4329–4336, 2024.
- [4] Z. Xu, B. Chen, X. Zhan, Y. Xiu, C. Suzuki, and K. Shimada, "A vision-based autonomous uav inspection framework for unknown tunnel construction sites with dynamic obstacles," *IEEE Robotics and Automation Letters*, vol. 8, no. 8, pp. 4983–4990, 2023.
- [5] B. Yamauchi, "A frontier-based approach for autonomous exploration," in *Proceedings 1997 IEEE International Symposium on Computational Intelligence in Robotics and Automation CIRA'97. 'Towards New Computational Principles for Robotics and Automation'*, 1997, pp. 146–151.
- [6] B. Zhou, Y. Zhang, X. Chen, and S. Shen, "Fuel: Fast uav exploration using incremental frontier structure and hierarchical planning," *IEEE Robotics and Automation Letters*, vol. 6, no. 2, pp. 779–786, 2021.
- [7] C. Cao, H. Zhu, H. Choset, and J. Zhang, "Tare: A hierarchical framework for efficiently exploring complex 3d environments," in *Proceedings of Robotics: Science and Systems (RSS '21)*, July 2021.

- [8] T. Dang, F. Mascarich, S. Khattak, C. Papachristos, and K. Alexis, "Graph-based path planning for autonomous robotic exploration in subterranean environments," in *2019 IEEE/RSJ International Conference on Intelligent Robots and Systems (IROS)*, 2019, pp. 3105–3112.
- [9] B. Zhou, H. Xu, and S. Shen, "Racer: Rapid collaborative exploration with a decentralized multi-uav system," *IEEE Transactions on Robotics*, vol. 39, no. 3, pp. 1816–1835, 2023.
- [10] A. Bircher, M. Kamel, K. Alexis, H. Oleynikova, and R. Siegwart, "Receding horizon "next-best-view" planner for 3d exploration," in *2016 IEEE International Conference on Robotics and Automation (ICRA)*, 2016, pp. 1462–1468.
- [11] D. Duberg and P. Jensfelt, "Ufoexplorer: Fast and scalable sampling-based exploration with a graph-based planning structure," *IEEE Robotics and Automation Letters*, vol. 7, no. 2, pp. 2487–2494, 2022.
- [12] L. Schmid, M. Pantic, R. Khanna, L. Ott, R. Siegwart, and J. Nieto, "An efficient sampling-based method for online informative path planning in unknown environments," *IEEE Robotics and Automation Letters*, vol. 5, no. 2, p. 1500–1507, Apr. 2020. [Online]. Available: <http://dx.doi.org/10.1109/LRA.2020.2969191>
- [13] A. Akbari and S. Bernardini, "Informed autonomous exploration of subterranean environments," *IEEE Robotics and Automation Letters*, vol. 6, no. 4, pp. 7957–7964, 2021.
- [14] Z. Xu, C. Suzuki, X. Zhan, and K. Shimada, "Heuristic-based incremental probabilistic roadmap for efficient uav exploration in dynamic environments," in *2024 IEEE International Conference on Robotics and Automation (ICRA)*, 2024, pp. 11 832–11 838.
- [15] B. Lindqvist, A. Patel, K. Löfgren, and G. Nikolakopoulos, "A tree-based next-best-trajectory method for 3-d uav exploration," *IEEE Transactions on Robotics*, vol. 40, pp. 3496–3513, 2024.
- [16] S. Geng, Z. Ning, F. Zhang, and B. Zhou, "Epic: A lightweight lidar-based aav exploration framework for large-scale scenarios," *IEEE Robotics and Automation Letters*, vol. 10, no. 5, pp. 5090–5097, 2025.
- [17] S. Yang and S. Scherer, "Cubeslam: Monocular 3-d object slam," *IEEE Transactions on Robotics*, vol. 35, no. 4, pp. 925–938, 2019.
- [18] L. Nicholson, M. Milford, and N. Sinderhauf, "Quadricslam: Dual quadrics from object detections as landmarks in object-oriented slam," *IEEE Robotics and Automation Letters*, vol. 4, no. 1, pp. 1–8, 2019.
- [19] X. Liu, J. Lei, A. Prabhu, Y. Tao, I. Spasojevic, P. Chaudhari, N. Atansov, and V. Kumar, "Slideslam: Sparse, lightweight, decentralized metric-semantic slam for multi-robot navigation," 2024. [Online]. Available: <https://arxiv.org/abs/2406.17249>
- [20] A. Rosinol, A. Violette, M. Abate, N. Hughes, Y. Chang, J. Shi, A. Gupta, and L. Carlone, "Kimera: From slam to spatial perception with 3d dynamic scene graphs," *The International Journal of Robotics Research*, vol. 40, no. 12-14, pp. 1510–1546, 2021.
- [21] X. Chen, A. Milioto, E. Palazzolo, P. Giguère, J. Behley, and C. Stachniss, "Suma++: Efficient lidar-based semantic slam," in *2019 IEEE/RSJ International Conference on Intelligent Robots and Systems (IROS)*, 2019, pp. 4530–4537.
- [22] X. Lei, T. Kim, N. Marchal, D. Pastor, B. Ridge, F. Schöller, E. Terry, F. Chavez, T. Touma, K. Otsu, B. Morrell, and A. Agha, "Early recall, late precision: Multi-robot semantic object mapping under operational constraints in perceptually-degraded environments," in *2022 IEEE/RSJ International Conference on Intelligent Robots and Systems (IROS)*, 2022, pp. 2017–2024.
- [23] L. Wellhausen and M. Hutter, "Rough terrain navigation for legged robots using reachability planning and template learning," in *2021 IEEE/RSJ International Conference on Intelligent Robots and Systems (IROS)*, 2021, pp. 6914–6921.
- [24] W. Xu, Y. Cai, D. He, J. Lin, and F. Zhang, "Fast-lto2: Fast direct lidar-inertial odometry," *IEEE Transactions on Robotics*, vol. 38, no. 4, pp. 2053–2073, 2022.
- [25] A. Chharia, T. Ren, T. Furuhashi, and K. Shimada, "Safe-construct: Redefining construction safety violation recognition as 3d multi-view engagement task," 2025. [Online]. Available: <https://arxiv.org/abs/2504.10880>
- [26] N. Ravi, V. Gabeur, Y.-T. Hu, R. Hu, C. Ryali, T. Ma, H. Khedr, R. Rädle, C. Rolland, L. Gustafson, E. Mintun, J. Pan, K. V. Alwala, N. Carion, C.-Y. Wu, R. Girshick, P. Dollár, and C. Feichtenhofer, "Sam 2: Segment anything in images and videos," *arXiv preprint arXiv:2408.00714*, 2024. [Online]. Available: <https://arxiv.org/abs/2408.00714>